ORIGINAL PAPER

Factors controlling reaction pathways during fluid–rock interactions

Lorena H. Filiberto[1] · Christine V. Putnis[1,2] · Maude Julia[1]

Abstract

Potential fluid pathways for fluid–rock interactions and the factors controlling these pathways have been investigated experimentally by simulating hydrothermal conditions, using sample cubes of Carrara Marble (calcite) and an anorthosite (plagioclase) rock in different solutions (pure water, sodium chloride, artificial seawater, sodium phosphate and sodium silicate) at 200 °C. Analytical techniques including SEM, Raman Spectroscopy, atomic force microscopy, and Electron Microprobe Analysis were used to characterize fluid-induced reactions. Results show aqueous fluids can penetrate grain boundaries within rocks and, dependent on fluid and solid compositions, coupled replacement reactions can occur. The available fluid volume for the reaction in a grain boundary versus the bulk fluid can influence replacement reaction pathways. When 0.1 M Na_2HPO_4 was used with Carrara Marble, or a Na-silicate solution was used with anorthosite, the replacement of calcite by hydroxylapatite or labradorite by albite, respectively, occurred along the grain boundaries of both rock types. In the experiments using seawater, the replacement of calcite by Mg-carbonates occurred predominantly from the sides of the cube samples and the grain boundaries were minimally affected within the timescale of the experiments (1–3 months). With 1 M Na_2HPO_4, hydroxylapatite precipitated both along the marble grain boundaries and the sample sides. Models based on experimental observations and PhreeqC simulations highlight the importance of grain boundaries and interconnected porosity in fluid-induced reactions. Such factors play an important role in the kinetics and relative solubilities of rock systems by changing the conditions at the interfacial fluid–mineral boundary layer that will determine initial dissolution or precipitation and whether the supersaturation of a product phase is reached.

Keywords Fluid pathways · Grain boundaries · Replacements · Calcite · Plagioclase · Dissolution–precipitation

Introduction

Aqueous fluids have long been known to be ubiquitous in the crust of the Earth (Fyfe 1978). How these fluids move through solid rocks has been the subject of research for many years (Putnis 2021 and references therein). Fluid pathways allowing access of aqueous fluids within rocks will include fractures, fault planes, grain boundaries, and interconnected pores enabling fluids to penetrate through originally nominally solid rocks (Ruiz-Agudo et al. 2014; Kruhl et al. 2013).

Once aqueous fluid is in contact with rock-forming minerals, these will enter an enhanced disequilibrium state initiating mineral dissolution and mineral-fluid reactions that may result in precipitation, replacement reactions (Putnis and Putnis 2007; Xia et al. 2009; Ruiz-Agudo et al. 2014; Putnis and Ruiz-Agudo 2021), element mobilization and mass transport (Hövelmann et al. 2010; Niedermeier et al. 2009), ore deposit formation (Brugger et al. 2016), and changes in stress distribution. The consequences of these reactions are far-reaching and involve many of the chemical and physical processes occurring in the Earth as reviewed by Putnis (2021). The driving force for these reactions is a chemical disequilibrium between the minerals and the aqueous fluid phase (Etschmann et al. 2014). Even the most insoluble mineral will start to dissolve in an aqueous solution releasing its component ions to an interfacial mineral-fluid boundary layer (Ruiz-Agudo et al. 2014; Putnis and Ruiz-Agudo 2021).

As previous studies demonstrate, mineral-fluid reactions might also lead to the development of new fluid pathways. Putnis and Putnis (2007) give examples of such reactions showing that the generation of an interconnected porosity in the product phase is a necessary condition for such a mechanism, as it allows fluid to maintain contact with a reaction interface which moves through the parent phase from the original surface. Jonas et al. (2014) and Pedrosa et al. (2016) also show how a pseudomorphic mineral replacement might produce intracrystalline porosity in the product phase allowing the reaction front to propagate towards the grain core. In all examples, the reaction is controlled by an interface-coupled dissolution–precipitation mechanism (Putnis and Putnis 2007; Ruiz-Agudo et al. 2014). Whether or not a replacement reaction proceeds depends on two main factors: the molar volume changes between parent mineral and product phase; and the solubility differences (or thermodynamic stability) between parent and product (Pollok et al. 2011). Experiments have shown that the latter consideration seems to be more important in the control of a pseudomorphic replacement reaction (Putnis et al. 2007). However, pseudomorphic replacements that produce a higher molar volume product phase may still occur but may induce stress in the rock at the replacement interface and therefore, reaction-induced fracturing and/or dislocations (Jamtveit et al. 2009; Niedermeier et al. 2009; Putnis et al. 2007; Plümper et al. 2012).

Other studies focus on the influence of the initial conditions that lead to these reactions such as original conductivity (Uno et al. 2022), initial fluid composition and the difference in reaction rates between types of fluid pathways (Pedrosa et al. 2016).

The term microreactors, presented by Etschmann et al. (2014), describe the concept of reactive fluid flow in small spaces within rocks, in this case grain boundaries, hosting an infiltrating fluid, where the saturation of a new product phase might be quickly achieved as the parent phase dissolves and reacts with the confined fluid. In this scenario, dissolution of a parent mineral may be coupled with the precipitation of a new product phase (Putnis and Putnis 2007; Ruiz-Agudo et al. 2014). Using rock sample cubes instead of single mineral grains in our experiments, the solid rock was both exposed to a fluid able to infiltrate within and along grain boundaries and to the bulk fluid around the external surfaces of the cubes. To compare with a natural scenario, a rock in contact with the bulk fluid inside the containers of the experiments might be equivalent to bodies of rocks near wide open fractures filled by aqueous fluids.

In this paper, we discuss experiments that show the importance of grain boundaries, how these allow fluid infiltration and what are the key variables that control the evolution of fluid pathways in rocks. To do so, we simulated hydrothermal conditions in laboratory experiments at 200 °C, for different periods of time and using different monomineralic types of rocks: Carrara Marble where calcite, $CaCO_3$, is the main phase; and an anorthosite with plagioclase, $(Ca_{0.6}Na_{0.4})Al_{1.6}Si_{2.4}O_8$, as the main component. Samples of these rocks were added in reactors with different solutions. Both the rocks tested have experienced metamorphic conditions and are composed of compacted grains with tight grain boundaries that nevertheless allow for a pathway for potential aqueous fluid infiltration. Previous research has centered on grain boundary migration and the significance of grain boundary reactions (Etschmann et al. 2014; Jonas et al. 2014; Pedrosa et al. 2017) but not in a comparative view of different mineralogies, chemistry and fluid composition.

Both minerals, calcite and plagioclase, are common rock-forming minerals in the Earth's crust. Due to the high solubility of calcite, replacement reactions occur at fast rates at relatively low temperatures when in contact with aqueous fluids (e.g., Etschmann et al. 2014; Jonas et al. 2014; Pedrosa et al. 2017; Julia et al. 2023). On the other hand, reactions involving plagioclase as the starting material are slower in comparison (Drüppel and Wirth 2018; Hövelmann et al. 2010; Niedermeier et al. 2009), however, reactions are seen on observable time scales of weeks and months. Calcite in the form of limestone and marble comprises large portions of exposed rocks. The significance of plagioclase feldspar as an important rock-forming mineral, in crustal processes, such as albitization associated with ore deposits, indicates its relevance (e.g., Kish and Cuney 1981; Oliver et al. 2004; Smith et al. 2007; Zhao and Zhou 2011).

Methods

Starting materials

Sample cubes ranging from approximately 3 to 4 mm^3 were cut (without using water) from two different rock types: an anorthosite rock from the Bergen Arcs in Norway; and a marble from Carrara, Italy (Fig. 1). Electron microprobe analysis (EMPA) gives an almost pure calcite composition for the Carrara Marble, $(Ca_{0.98}Mg_{0.02})CO_3$ (Table 1), with an average grain size of 300 μm. From electron backscatter diffraction (EBSD) analysis (Petráňová et al. 2016), there is no preferred crystallographic orientation in Carrara Marble. The exact composition of the original plagioclase sample (labradorite, $Ca_{0.6}Na_{0.4}Al_{1.6}Si_{2.4}O_8$) was determined through electron microprobe analysis (Table 2). The plagioclase had an average grain size of 600 μm.

Grain boundaries on the anorthosite sample were sometimes partially filled with tiny biotite, aluminum silicate and anorthite grains of < 10 μm size, especially when some garnet crystals (200–500 μm) were present. The original Carrara Marble samples had some minor porosity and the

Fig. 1 SEM Back Scatter Electron (BSE) images of the starting material. **a** Carrara Marble cube section; MR0. **b** Carrara Marble detail showing the grain boundaries between the calcite grains. **c** Anorthosite rock cube section; PL0. **d** Anorthosite rock detail showing the grain boundaries between the labradorite grains. **e** Grain boundaries filled by anorthosite (An) and kyanite (Ky) in the anorthosite rock. *Grt* Garnet
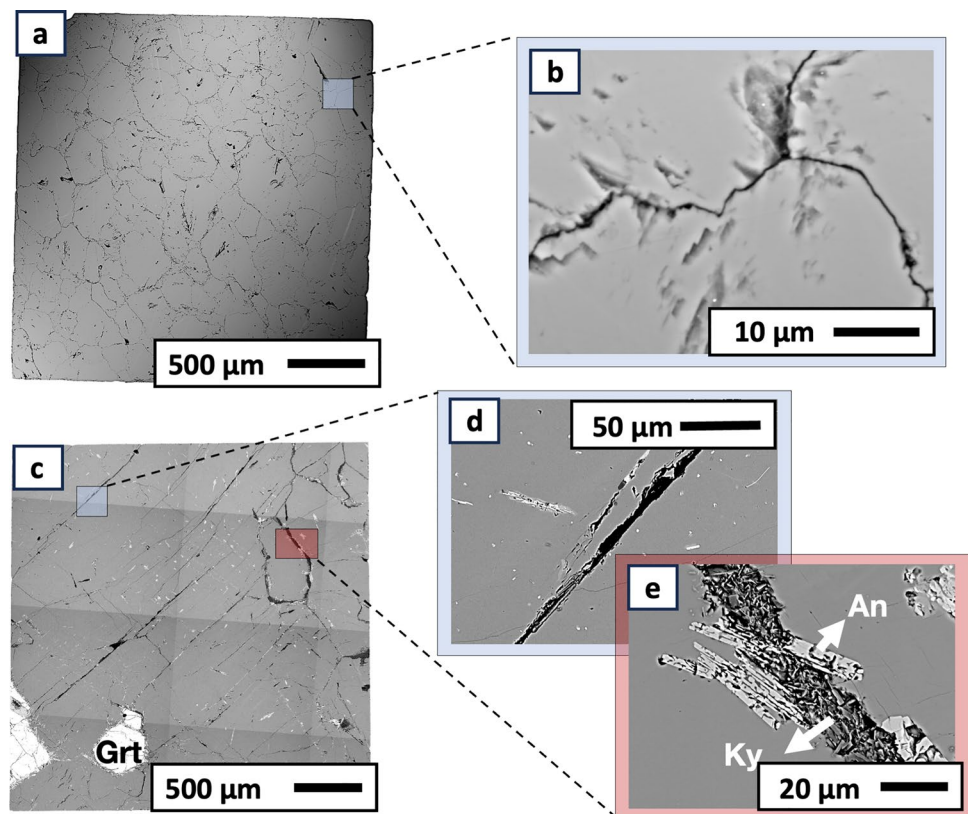
tight grain boundaries (< 0.5 μm) were clearly visible in electron backscattered (BSE) images.

The sample rock cubes were reacted using different solutions under hydrothermal conditions: 200 °C at autogenous pressure; and for varying periods of time: 5 to 80 days for the calcite samples and 1 to 3 months for the plagioclase samples. The solutions used for the calcite experiments were: deionized water pH 6.8; artificial seawater (0.42 M NaCl, 0.05 M $MgCl_2$, 0.03 M Na_2SO_4, 0.01 M $CaCl_2$, 0.01 M KCl, 0.0024 M $NaHCO_3$, 0.0008 M KBr, 0.0004 M H_3BO_3, 0.0001 M NaF) pH 7.7; 0.1 M and 1 M sodium phosphate pH 8.6 and pH 9.1, respectively; 1 M and 2 M NaCl pH 7.1 and pH 6.8, respectively. For the plagioclase experiments, as well as pure water, a NaCl solution, artificial seawater (same compositions as for the marble experiments), and a sodium silicate solution pH 10.5 were used. All solutions were made using doubly deionized water (resistivity > 18 mΩ cm) and reagent grade solids (Sigma Aldrich). The pH for every solution was measured at room temperature (~ 22 °C) using WTW InoLab pH-meter. All experiments were made in duplicate and experiments were repeated if similar results were not achieved in repeated experiments. A summary of the solutions and methods is shown in Table 3 for the experiments including Carrara Marble and the anorthosite rock. Data for the duplicate experiments can be found in the Online

Resource 1. The tables also include the initial pH of the solutions at 200 °C calculated with PhreeqC (Parkhurst and Appelo 1999).

Molar volume changes were calculated using mineral densities and without including significant changes in porosity during the reactions, the latter would effectively decrease the density and hence increase the volume.

Experimental setup

Each sample cube was weighed and then added together with 2 ml of the solution into Teflon reactors previously introduced into steel autoclaves, then sealed to prevent fluid loss during the experiments, and finally inserted into the furnace where the hydrothermal conditions were simulated. After the experiments were completed, the enclaves were quickly quenched (within a couple of minutes) using pressured air. The solutions were sealed and later analyzed using inductively coupled plasma optical emission spectrometry (ICP-OES). The cubes were gently dried, using filter paper and weighed again. To analyze the reactions, the cubes were mounted in epoxy resin and sectioned through the center for analysis using scanning electron microscopy (SEM; JEOL JSM-6610LV) equipped with energy-dispersive X-ray analysis (EDX).

Table 1 Plagioclase microprobe analysis of the anorthosite experiments

Solution	1	2	3	4
	Sodium silicate			Seawater
SiO_2	53.38	67.96	65.63	52.09
Al_2O_3	28.55	19.99	21.57	29.51
FeO	0.04	*b.d*	0.04	0.09
CaO	11.68	0.74	2.70	12.03
Na_2O	4.80	10.99	9.58	4.50
K_2O	0.12	0.02	0.06	0.11
Total	98.57	99.78	99.61	98.38
Numbers of ions on the basis of 8 O				
Si	2.447	2.976	2.890	2.398
Al	1.543	1.031	1.120	1.601
Fe^{2+}	0.002	*b.d*	0.001	0.004
Ca	0.574	0.035	0.127	0.594
Na	0.427	0.933	0.818	0.402
K	0.007	0.001	0.003	0.006
Ab	0.42	0.96	0.86	0.40
An	0.57	0.04	0.14	0.59
Or	0.01	0.00	0.00	0.01

bd below detection limit

1. Average composition of the labradorite in the anorthosite sample that reacted for 3 months with a sodium silicate solution; PL8

2. Albite core replacing the labradorite in 1; PL8

3. Albite rim replacing the labradorite in 1; PL8

4. Average composition of the labradorite in the anorthosite sample that reacted for 3 months with seawater; PL5

Electron microprobe analysis

For quantitative analysis and element mapping, the samples were analyzed using an electron microprobe (JEOL JXA-8530F), equipped with wavelength dispersive X-ray spectrometer (WDS) and an energy dispersive X-ray spectrometer (EDS). A total of 20 spot analyses for the plagioclase and 60 for the carbonates were performed using an accelerating voltage of 15 kV, an electron beam current of 4 nA, and a probe diameter of 5 μm. Element mapping was performed using 15 kV, 40 nA of beam current, and a probe diameter of 0.3 μm. Analytical errors are estimated to be on the order of $\pm$ 1–2%.

Raman spectroscopy

Raman spectra were collected using a Horiba XploRA Raman-Spectrometer equipped with a laser source of 632.85 nm. A $100 \times$ objective on a confocal microscope was used to focus the laser on the sample surface. The acquisition time for each spectrum was 30 s, and 2 spectra were collected for each of the replacement phases. Baseline correction was performed using the software OriginPro and the spectra were then compared to a database of known mineral spectra to identify the mineral composition of the sample. To include the main phosphate and carbonate vibration modes the spectra were recorded between 100 and 1500 cm^{-1} frequency, and between 2900 and 3900 cm^{-1} to allow OH detection.

Atomic force microscopy (AFM)

A pure calcite crystal was cleaved along the {01–14} direction to produce a calcite surface approx. 3×2 mm and 1 mm thick and attached to a Teflon™ sample holder with non-reactive conductive carbon cement (Plano LeitC), immediately prior to experiments. In-situ experiments were performed in a fluid cell of a Bruker Nanoscope III Multimode AFM working in contact mode at ambient temperature (22 ± 1 °C) using gold coated AFM tips (NuNano SCOUT 70 RAu). Pure water (doubly deionized, resistivity > 18 mΩ cm) was injected into the cell through a tube connected to a syringe. Pure water was flowed over the calcite surface for 10 scans (approx. 1 min per ´scan at a scan rate of 3.5 Hz). The calcite surface was subsequently allowed to remain in static water. Further in situ scans were made after 1 h, 3 h and 24 h.

PhreeqC simulations

Simulations of potential reactions were made using the *SIT* database for reactions involving sodium phosphate solutions, the *minteq.v4* database for seawater systems, and the *PHREEQC* database for the other systems, within the Phreeqc program (Parkhurst and Appelo 1999). High ionic strengths, phases available and compatibility with other phases not included in the original databases were the factors considered for the database selection. The main aim of these simulations was to compare the difference in saturation indices of the different potential phases, when using a volume of water that reflects the bulk solution (2 ml) and when using a volume of water that corresponds with a fluid in a grain boundary (1 μm). Our experimental observations influenced the simulation inputs. Input scripts can be found in the Online Resource 2.

For the Carrara Marble with Na_2HPO_4 solutions and the anorthosite rock with Na-silicate solutions, simulations were made by dissolving a 1 nm wide layer of the parent phase both around the cube and in a 1 μm wide grain boundary. Calcite and labradorite molar volumes were used to calculate the number of moles of each mineral that would be in this layer. For the seawater experiments with Carrara Marble, 1% of the total number of moles of calcite in the cube were dissolved. The effects of dissolving a layer of calcite and a

Table 2 Electron microprobe analysis of the Carrara Marble experiments reacting for 80 days with different solutions at 200 °C

Solution	1	2	3	4	5	6	7	8
	–	Pure water	1 M NaCl	0.1 M Na$_2$HPO$_4$	Artificial seawater			
Na$_2$O	0.01	0.01	b.d	0.02	0.02	0.04	0.03	0.41
Cr$_2$O$_3$	0.05	0.02	b.d	0.03	0.02	0.02	0.01	0.03
FeO	0.06	0.06	b.d	0.02	0.00	0.04	0.07	0.02
MnO	0.01	0.02	b.d	0.01	0.02	0.01	0.03	0.02
MgO	0.65	0.70	0.89	0.74	0.86	42.58	68.35	19.73
CaO	56.26	58.70	57.68	58.12	56.60	5.99	0.30	34.12
SrO	0.05	*b.d*	b.d	0.03	0.07	*b.d*	0.02	*b.d*
BaO	0.01	0.00	0.01	0.02	0.01	0.03	0.03	0.02
CO$_2$	42.91	40.50	41.42	41.02	42.26	51.28	31.16	46.04
Total	100.01	100.01	100	100.01	99.86	99.99	100	100.39
Numbers of ions on the basis of 6 O								
Mg	0.033	0.036	0.045	0.040	0.043	1.814	3.263	0.919
Fe^{2+}	0.002	0.002	b.d	0.001	0.000	0.001	0.002	0.000
Mn	0.000	0.001	b.d	0.000	0.001	0.000	0.001	0.001
Ca	2.026	2.163	2.104	2.130	2.052	0.183	0.010	1.142
Sr	0.001	b.d	b.d	0.001	0.002	*b.d*	0.000	0.002
Ba	0.000	0.000	0.000	0.000	0.000	0.000	0.000	0.000
Na	0.000	0.000	b.d	0.001	0.001	0.001	0.001	0.001
Cr	0.001	0.000	b.d	0.000	0.000	0.000	0.000	0.000

b.d. below detection limit

1. Average composition of the original calcite grains in Carrara Marble (unreacted sample); MR0

2. Average composition of calcite grains after experiments with a pure water solution; MR4

3. Average composition of calcite grains after experiments with a 1 M NaCl solution; MR9

4. Average composition of calcite grains after experiments with a 0.1 M Na$_2$HPO$_4$ solution; MR20

5. Average composition of calcite grains after experiments with an artificial seawater solution; MR15

6. Magnesite replacing calcite after experiments with an artificial seawater solution; MR16

7. Brucite–magnesite mixture replacement after experiments with an artificial seawater solution; MR16

8. Dolomite as a replacement product after experiments with an artificial seawater solution; MR16

layer of hydromagnesite in a grain boundary where these two phases are in contact were also tested.

Image analysis

Textural analysis of the resulting sectioned cubes was performed with the use of the image analysis software JMicroVision v1.3.2 (Roduit 2023). Porosity was obtained through the "Object Extraction" tool, producing a percentage of the area of the BSE image containing black pixels that will represent the grain boundaries, pores and, cracks of the sample. All analyzed images were previously enhanced using the same steps to ensure all grain boundaries will reach the minimum threshold to be considered as porosity. The software was also used to measure the average replacement width and the average grain size of the starting materials.

Table contains data for the first set of experiments, which are representative enough of the results. Duplicate experiments data can be found in Online Resource 1.pH (200°):

Data obtained from PhreeqC simulations (Online Resource 2).

Porosity: Porosity estimation (including grain boundaries, cracks, and pores) using the image analysis software JMicroVision after BSE images.

Results

Solid materials

Carrara marble

Carrara marble with pure water and NaCl solutions When compared to an unreacted sample, the calcite composition remains unchanged, and neither the deionized water nor the 1 M NaCl solution produced any compositional changes nor ion-exchange replacement reactions. EDX and microprobe analyses reveals no significant change in the Ca/Mg ratio within the samples (Table 2).

Table 3 Summary of the hydrothermal experiments performed at 200 °C, using 2 ml of solution and with a cubic rock sample of ~ 27 mm^3

Starting material		Carrara Marble (MR)		Calcite					
Label	Solution	Time (days)	pH (25 °C)	pH (200 °C)	Replacement product	Porosity (%)	Average replacement width	Textural observations	
MR0	–	–	–	–	–	0.57	–	–	
MR1	Pure water	5	6.8	5.2	–	0.89	–	Grain boundaries become wider after 10 and 20 days, then tighter after 40 days and wider again after 80 days	
MR2		10				1.01			
MR3		20				1.57			
MR4		40				0.98			
MR5		80				1.35			
MR6	1 M NaCl	5	7.1	5.1	–	2.34	–	Grain boundary opening	
MR7		10				1.98			
MR8		20				2.23			
MR9		40				2.05			
MR10		80				1.95			
MR11	2 M NaCl	5	7.1	5	–	2.02	–	Grain boundary opening	
MR12	Seawater	5	7.7	5.7	–	0.98	–	–	
MR13		10			–	4.87	–	Grain boundary opening	
MR14		20			Magnesite	2.41	10 μm	Grain boundary tighter, replacement from the sides of the cube. Ca-sulphate precipitation on the sides and pores	
MR15		40			Magnesite, brucite, and dolomite	1.75	18 μm		
MR16		80				1.05	28 μm		
MR17	0.1 M Na$_2$HPO$_4$	5	8.6	7	Hydroxylapatite	0.47	1.8 μm	Replacement along the grain boundaries	
MR18		10				0.56	2.6 μm		
MR19		20				0.39	1.7 μm		
MR20		40				0.44	1.8 μm		
MR21		80				0.47	2.3 μm		
MR22	1 M Na$_2$HPO$_4$	5	9.1	8.2	Hydroxylapatite	0.52	12 μm	Replacement from the sides of the cube and along the grain boundaries	

Starting material		Anorthosite (PL)		Labradorite				
Label	Solution	Time (days)	pH (25 °C)	pH (200 °C)	Replacement product	Porosity (%)	Average replacement width	Textural observations
PL0	–	–	–	–	–	0.88	–	–
PL1	Pure water	90	6.8	5.2	–	0.91	–	–
PL2	1 M NaCl	90	7.1	5.1	–	1.05	–	–
PL3	Seawater	30	7.7	5.7	–	2.56	–	Grain boundary opening
PL4		60				3.01	–	
PL5		90				4.98		
PL6	Na-silicate	30	10.5	8.6	–	1.01	–	–
PL7		60			–	0.99	–	–
PL8		90			Albite	1.28	2 μm	Replacement along the grain boundaries

Grain boundaries in the samples appeared wider (ΔWidth = ~ 0.5 μm) after experiments in pure water and NaCl solutions, but there is no consistent observable widening increase over time. To the contrary, grain boundaries appeared tighter again after 40 days in solution and in pure water grain boundaries widen to previous levels after 80 days (Fig. 2).

The experiments where a 2 M NaCl solution was used did not produce any significant changes after 5 days when compared with the ones where a 1 M NaCl solution was used for the same period of time.
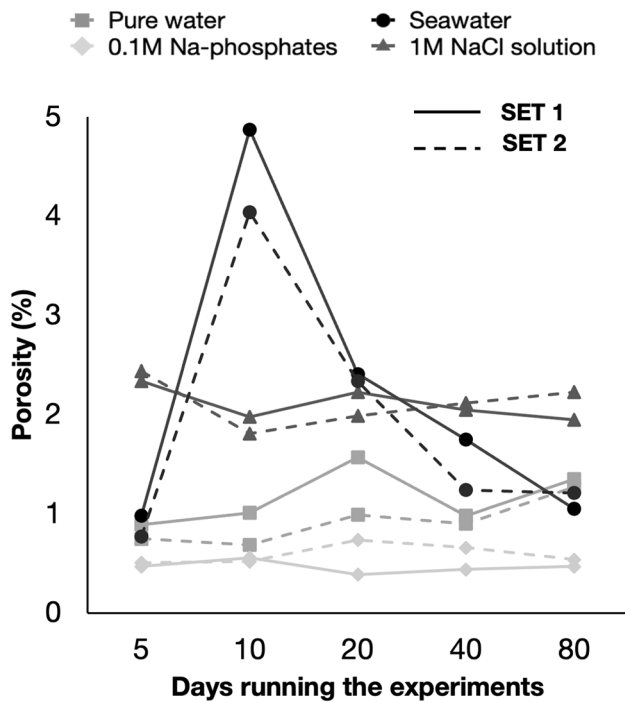
Carrara marble in artificial seawater solution EDX analysis showed a Mg-rich phase replacing calcite after the first 20 days of Carrara Marble in artificial seawater solution (Fig. 3b). When the experiments ran for less than 20 days, only dissolution in the widening of grain boundaries was observed (Figs. 2, 3a). After 20 days the replacement of calcite by the Mg-rich phase occurs from the sides of the Carrara Marble cube and progresses very slowly along the calcite grain boundaries (Fig. 3c, d).

Electron microprobe analysis suggests that it is a Mg-carbonate, most likely magnesite or a hydrated magnesite (Table 2). This replacement continuously progresses with time. Dolomite (or a $Ca_{0.5}Mg_{0.5}CO_3$ phase) appears in some places of the cube as an intermediate phase between the calcite and the magnesite, while in other areas a phase richer in Mg than the magnesite is also present (Figs. 3d, 4a, b). The progression of MgO mol% and CaO mol% through the replacement products is shown in Fig. 5, as well as the evolution of the water content along this replacement that was observed by the OH peak intensity in the Raman analysis (Online Resource 3).

A gap is also visible in the calcite-magnesite interface but not between the dolomite with any of the other phases. Porosity is already visible at the micron scale in the magnesite but not observed in the dolomite. Some of these gaps are filled with a calcium sulphate phase which is also visible growing on the sides of the cube (Fig. 3b–d).

Fig. 2 Porosity estimations (grain boundaries, pores and cracks) for the Carrara Marble experiments obtained with the JMicroVision software for image analysis. Data available in Table 3 and Online Resource 1. This porosity mainly reflects the widening or narrowing of the grain boundaries probably due to a dissolution effect

Fig. 3 SEM Back Scatter Electron (BSE) images of the observed experimental results at 200 °C of Carrara Marble samples with an artificial seawater solution. **a** 10 days, dissolution observed by the widening of grain boundaries; MR13. **b** 20 days, magnesite partially replaces the original calcite from the cube external surface; MR14. **c** 80 days, overview of the cube showing the replacement from the external sides of the cube and along grain boundaries; MR16. **d** Zoom in of **c**, blue square, where all the replacement phases are shown: magnesite, dolomite, brucite, and Ca-sulphate. Red square in **d** shows the area for element microprobe mapping in Fig. 4
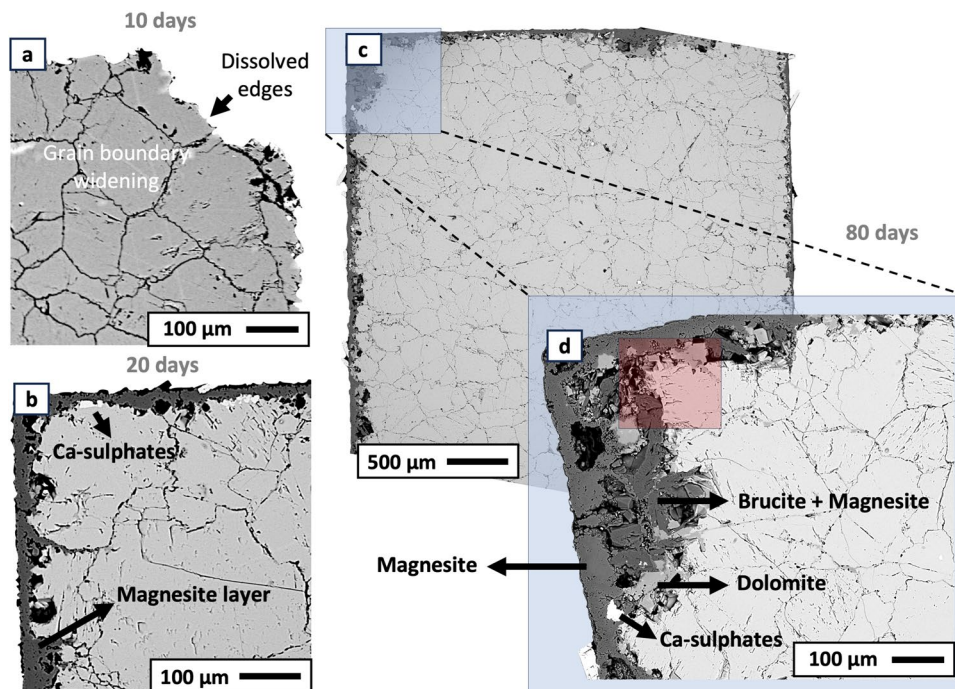
Fig. 4 **a–d** Electron Microprobe maps of the main replacement products in Carrara Marble. **a** and **b** calcium and magnesium contents, respectively, of the area marked in Fig. 3d from the Carrara Marble cube that reacted for 80 days with an artificial seawater solution; MR16. **c** and **d** calcium and phosphorus contents, respectively, of hydroxylapatite replacing the calcite along a grain boundary after reacting 80 days with a 0.1 M Na_2HPO_4 solution; MR21. **e–h** EDX maps of the replacement of labradorite (Lab) by albite (Ab) in the area marked in Fig. 6; PL8
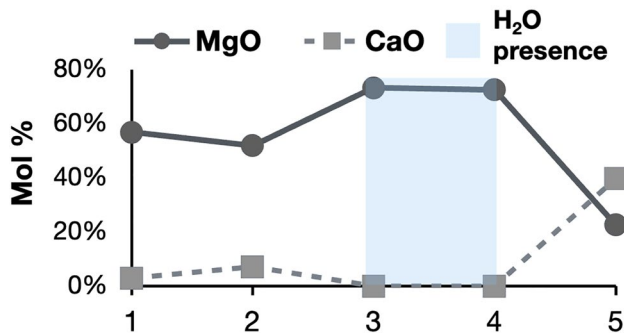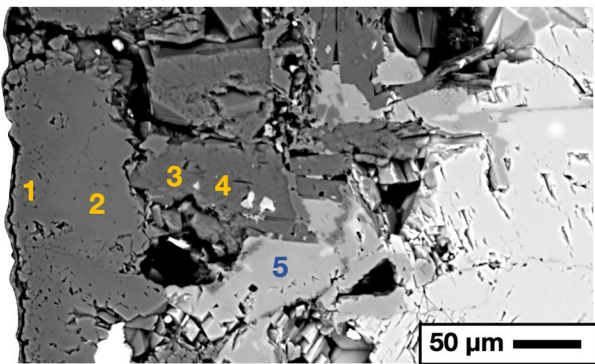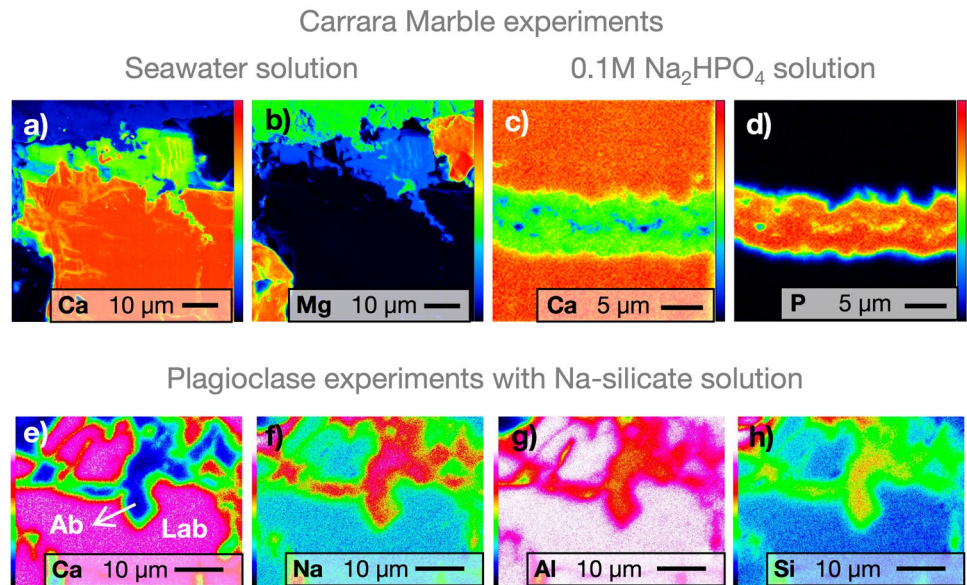
Fig. 5 MgO and CaO mol% changes in the replacement products of the experiment in which artificial seawater reacted with Carrara Marble for 80 days; MR16. Data obtained from EDX analysis

Carrara marble in a Na_2HPO_4 solution A new calcium phosphate phase replaces the calcite along the grain boundaries when using a 0.1 M Na_2HPO_4 solution (Fig. 6a, b). The replacement product is already visible after the first 5 days and was confirmed to be hydroxylapatite through

Raman analysis. The new product phase is highly porous and the pore size varies depending on how close it is to the grain boundary, with bigger pores close to the boundary and smaller pores next to the reaction front. A small size gap (1–2 μm) between the Ca-phosphate product phase and the original calcite is only visible after reacting with a 0.1 M Na_2HPO_4 solution for 80 days.

The phosphorus content in the product phase decreases from the grain boundary towards the reaction front while the Ca content increases, according to microprobe maps (Fig. 4c, d).

When using a 0.1 M Na_2HPO_4 solution, almost no replacement is observed at the edges of the cube, where the calcite was in contact with the bulk fluid and the cube maintains its original size. In this case, the replacement occurs exclusively along the grain boundaries and after 80 days the replacement affected more than 50% of the grain boundaries. With an increase in the solution concentration to 1 M Na_2HPO_4, a replacement was observed from the edges of the cube already after 5 days, as well as along the grain boundaries that were closer to the edge of the cube (Fig. 6c, d). In this case the porous replacement product continues even further into the calcite grains, leaving a finer porosity than in the experiments where a lower phosphate concentration was used.

When using the lower concentrated phosphate solution, the replacement does not occur in a consistent manner over time; in fact, the grain boundaries of the sample that reacted for 80 days appear to be less affected by a replacement reaction than those that reacted for shorter periods of time.
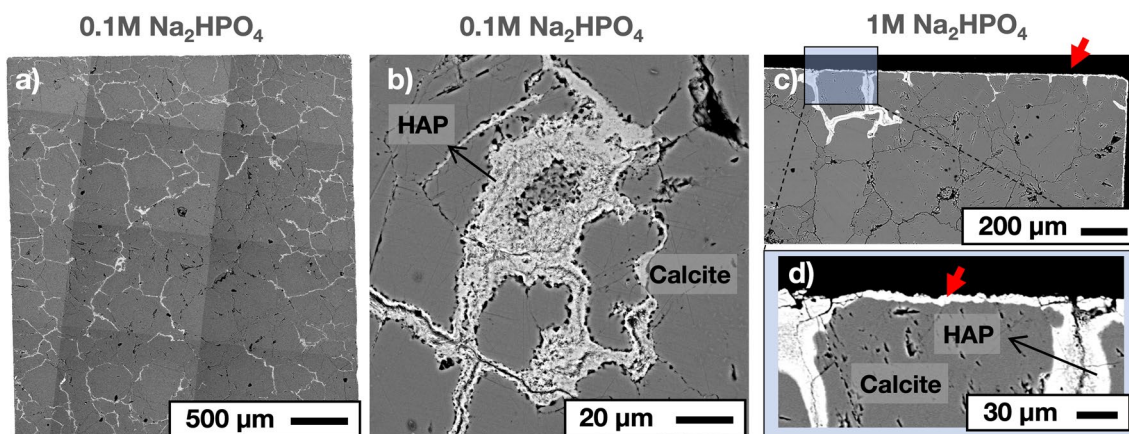
Fig. 6 SEM Back Scatter Electron (BSE) images of the observed experimental results at 200 °C of Carrara Marble samples with a sodium phosphate solution at different concentrations (0.1 M and 1 M). **a** 80 days, overview of the cube using 0.1 M Na_2HPO_4 solution showing the replacement along the grain boundaries (appears lighter); MR21. **b** 40 days, detail of the hydroxylapatite replacing the original calcite with a 0.1 M Na_2HPO_4 solution; MR20. **c** 5 days, hydroxylapatite replacing the calcite using a 1 M Na_2HPO_4 solution; MR22. **d** Zoom in of the marked blue square in **c**. Red arrows show that the replacement reaction is taking place also along the sides of the cube for the higher concentrated solution. Note the porosity in the replacement phase

Plagioclase anorthosite sample

Anorthosite with artificial seawater

Increasing dissolution over time was observed when the anorthosite cube samples reacted with the same artificial seawater composition as used for the Carrara Marble experiments. This feature is mainly observed with the strong widening of the grain boundaries (from ~0.5 μm to ~2 μm) and the slightly irregular edges. The weight of the cube also slightly decreases after 3 months reacting with the solution ($\Delta \text{Weight} = -0.0011$ g). No replacement product was identified during this reaction.

Anorthosite with Na-silicate solution

After three months of an almost monomineralic plagioclase rock sample mainly composed of anorthosite (~ $An_{0.58}Ab_{0.41}$, labradorite) reacting with a sodium silicate solution at 200 °C, a sodium richer plagioclase, almost albite ($An_{0.09}Ab_{0.91}$), starts replacing the labradorite (Fig. 7) along the grain boundaries. The amount of replacement was not consistent between runs. The albite grains show Na-poor rims and Na-rich cores, observed by the microprobe analysis (Table 1) and EDX maps (Fig. 4e–h).

The anorthosite samples showed no changes in both pure water and NaCl solutions within the time scale of the experiments–up to 3 months.
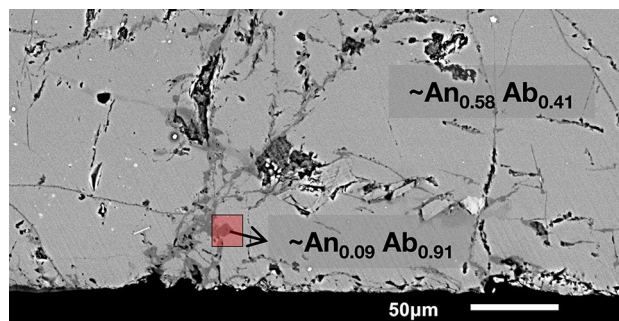

Fig. 7 SEM Back Scatter Electron (BSE) image of the replacement of labradorite by albite in the anorthosite rock sample with a Na-silicate solution after 3 months, showing an albite replacement product along grain boundaries (darker grey); PL8. Red square shows the area for EDX mapping in Fig. 4

Fluid geochemistry

Figure 8 shows the changes in Ca^{2+} in solution over time when different types of solutions were used with Carrara Marble. The calcium content increases over time in artificial seawater, with a small decrease between 10 and 20 days, which corresponds to the first occurrence of the Mg-rich phase that is replacing the calcite. Despite the fact that the seawater solution was the only one with some initial calcium content, the experiments using this solution released the highest values of Ca^{2+} in solution from the solid phase after 10 days or more.

When deionized water is used, the pattern appears cyclical, with a decrease in Ca^{2+} in solution from 5 to 20 days, followed by an increase back to previous levels.
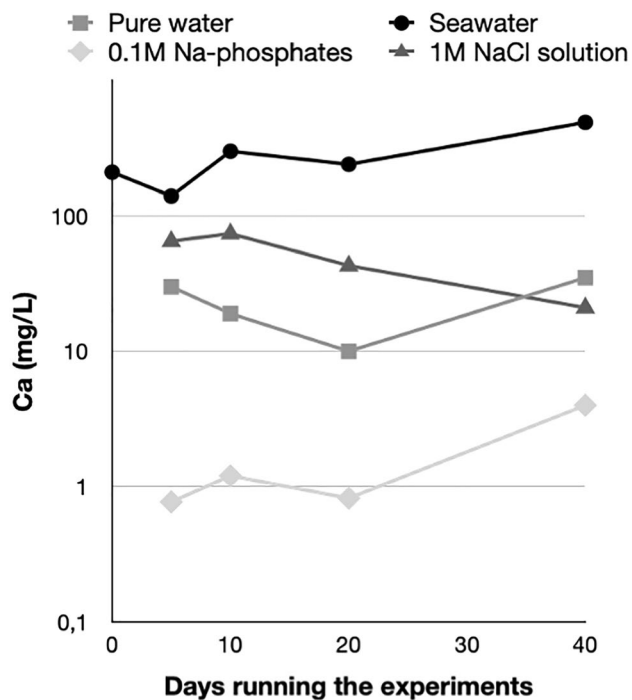
Fig. 8 Calcium content (ICP–OES analyses) in solution after running the experiments using Carrara Marble samples. The lowest Ca content is shown in experiments with a 0.1 M Na-phosphate solution as Ca was consumed in the formation of apatite. Calcium content variation in the pure water and NaCl solution could be related with calcite dissolution and reprecipitation. The seawater solution was the only one with initial calcium present

The fluid analyzed after the experiments with the sodium phosphates solution and Carrara Marble present the lowest contents of the Ca^{2+} in solution and follows a similar pattern as the ones with seawater, with an overall increase in calcium and a small decrease between 10 and 20 days.

With the anorthosite sample and the sodium silicate solution the analysis shows a consistent increase of Ca^{2+} in solution over time, with a major increase between 60 and 90 days when the first albite appears.

Raman spectroscopy

Characteristic Raman spectra for the carbonates and phosphates formed in the replacement reaction are shown in Online Resource 3.

For the samples where seawater was used after 80 days the following phases were recognized: dolomite, magnesite, and mixture of brucite and magnesite. Dolomite showed peaks at 174, 298, 325, 723, and 1096 cm^{-1}, associated with carbonate group vibrations, as well as symmetric stretching vibrations of the Ca–Mg bond and the bending vibration of the Mg–O bond. Magnesite exhibited peaks at 326 and 1093 cm^{-1}, related to the symmetric stretching and bending

vibrations of the carbonate group. The mixture of brucite with magnesite showed peaks at 280, 444, and 1092 cm^{-1}, which correspond to the bending vibration of the Mg–O bond in brucite, and the bending vibration and symmetric stretching of the carbonate group in magnesite. An OH peak was also observed at 3646 cm^{-1} corresponding to the brucite.

When using a Na-phosphate solution the replacement product was hydroxylapatite but despite using a small spot size to obtain the Raman spectra, peaks corresponding to a carbonate phase were also observed. This could either be an overlap with the calcite or CO_3 in the apatite structure (carbonate–hydroxylapatite). Peaks at 155, 281, 962, and 1086 cm^{-1} are associated with the bending vibration of the P–O bond in hydroxylapatite, bending vibration of the carbonate group in calcite, symmetric stretching vibration of the PO_4 group in hydroxylapatite, and symmetric stretching vibration of the carbonate group in calcite. This phase also presented an OH peak at 3571 cm^{-1}.

Atomic force microscopy experiments

Initially the calcite surface was observed dissolving by the nucleation and spreading of rhombohedral etch pits that were characteristically 1 unit cell deep (approx. 3.5 Å, or multiples thereof). After one, two and several hours in static water the calcite surface was observed to became increasingly covered with tiny nanoparticles (observable diameter 20–40 nm) presumably composed a Ca-carbonate, as no other ionic species were present. After 24 h under non-flow conditions the surface was further covered with nanoparticles, especially along step edges and etch pit edges—that is, in positions of faster dissolution (Fig. 9).

Discussion

Replacement mechanism

All the replacement reactions observed in the hydrothermal experiments, both at the surface of the sample rock cubes or along their grain boundaries, are characterized by two features: (1) a pseudomorphic replacement of a parent mineral by a new product phase, where the size of the cubes is preserved: and (2) the development of interconnected porosity in the product phase. Both are characteristics of an interface-coupled dissolution–precipitation mechanism (Putnis and Putnis 2007, 2022; Putnis et al. 2007) where dissolution of the parent phase must be achieved to supersaturate the fluid in the fluid–mineral interfacial boundary layer and hence to precipitate a new phase. This is accompanied by porosity development at a reaction interface that allows for the progression of the reaction front within a previously
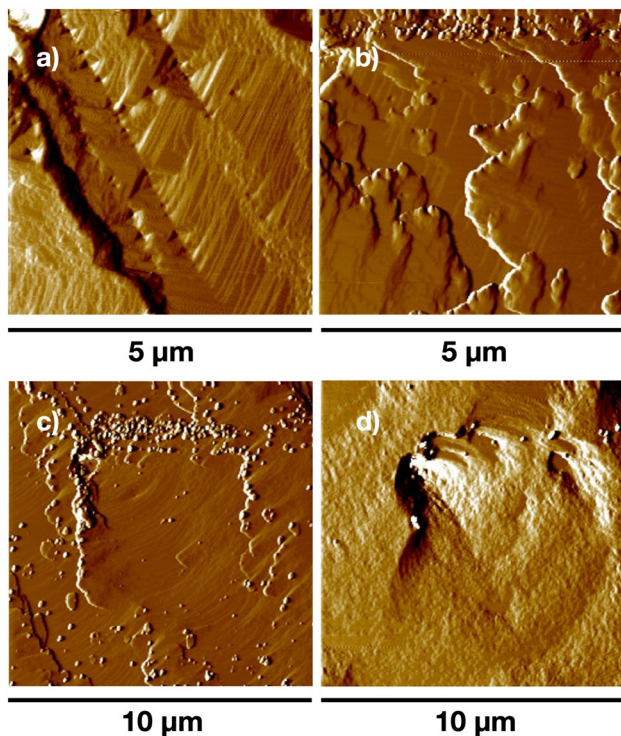
Fig. 9 Sequential AFM deflection images of calcite with pure water solution. The four images show the same sample's surface. **a** Calcite surface after 10 min in pure water flow showing dissolution. **b** After 1 h in static pure water. **c** After 3 h in static pure water. **d** After 24 h in static pure water. Note the calcite nanoparticles precipitating on the calcite's surface in **b–d**

solid mineral so that the reaction can proceed to result in a pseudomorphic replacement of a parent mineral (Etschmann et al. 2014; Janssen et al. 2010; Xia et al. 2009; Jonas et al. 2014; Pollok et al. 2011; Ruiz-Agudo et al. 2014).

Using ^{18}O-enriched aqueous solutions, previous studies have already shown that ^{18}O is incorporated in the new product phase, indicating that dissolution of the parent mineral must be coupled to the formation of a new phase (Hövelmann et al. 2010; Labotka et al. 2004; Niedermeier et al. 2009). These previous studies were conducted at high temperatures, > 600 °C and concomitant with metamorphic conditions. Our experiments are at a relatively low temperature (200 °C) more in line with diagenetic processes. Results of dissolution of the parent calcite (comprising Carrara Marble) or plagioclase occurred, driven by disequilibrium, to then precipitate a new phase enriched in ^{18}O.

A key feature of this mechanism is that on dissolution of the parent mineral a thin boundary layer at the fluid–mineral interface must quickly become supersaturated with a new phase. Diffusion of ions away from the mineral-fluid interface into the bulk fluid would reduce the concentration of these ions at the interface, so to achieve the replacement the precipitation rate must be faster than the diffusion rate of the

dissolved ions into the bulk fluid. This implies that the first rate-controlling factor is dissolution and consequently dissolution is coupled with the precipitation of a new phase at the reaction interface (Putnis and Putnis 2022; Ruiz-Agudo et al. 2014).

The effect of grain boundaries on calcite dissolution–reprecipitation

In the experiments when Carrara Marble was placed in pure water or NaCl solutions, after 5 days grain boundaries were seen to widen indicating dissolution which would enhance potential fluid infiltration. This phenomenon has been recently reported showing that the internal microstructure of rocks can significantly change reaction rates (Weber et al. 2023). Grain boundary widening could be also associated with a quenching effect resulting from the thermal stresses or from the rapid cooling process after the samples were removed from the furnaces (Petráňová et al. 2016; Raghami et al. 2020).

However, in our experiments after 40 days the grain boundaries become tighter again. From the Phreeqc modeling results (Online Resource 2), when using a solution volume that corresponds to a 1 μm wide grain boundary, instead of the 2 ml used in the original solution, calcite dissolution was reduced as the fluids were quickly supersaturated with calcite. According to the Ca^{2+} content present in the resulting solution after the experimental runs (Fig. 8), calcite dissolution was achieved at every experimental run to some extent. This difference in calcite dissolution might create a concentration gradient allowing Ca^{2+} and CO^{3-} ions to diffuse from the bulk fluid into the grain boundaries, producing calcite reprecipitation along the boundaries, which could be observed by the widening and narrowing of the grain boundaries with time. This hypothesis is corroborated by conducting AFM experiments and observing the precipitation of nanoparticles onto a dissolving calcite surface after several hours in pure water (Fig. 9). Additionally, the faster CO^{3-} diffusional coefficient with respect to Ca^{2+} ions could momentarily decrease the pH of the solution as it reaches the grain boundary interfacial solution, increasing calcite dissolution before the Ca^{2+} ions arrive to supersaturate the fluid again. Subsequently after precipitation of a new carbonate phase, the interfacial fluid would again become undersaturated and promote dissolution. This would emphasize the dynamic nature of the whole reaction process.

From ICP–OES analyses, initial calcite dissolution occurs (increase in Ca content) during the first 10 days of running the experiments with Carrara Marble and seawater (Fig. 3a) and then, from the decrease in Ca content, calcite reprecipitation might be also related to the grain boundary narrowing observed after 20 days (Fig. 3b) when the first layer of a Mg-phase replaces the calcite on external surfaces of

the cube and hinders ions from the external solution from reaching the internal grain boundaries.

Replacement reaction pathways

Fluids in rocks are often constrained into small (nm—µm-size) spaces, such as grain boundaries and pores. A restricted fluid volume might favor an increased ionic concentration at the mineral-fluid interface and therefore enhance potential reactions (Etschmann 2014). Hence, constrained fluids within grain boundaries would promote reactions through the coupling of dissolution and precipitation by the resulting simultaneous supersaturation of a new phase within the mineral-fluid boundary layer.

Dependent on the initial solution compositions used, dissolution of the parent phase (either calcite or plagioclase) was required to achieve supersaturation of the product phase and replace the original material.

Experimental observations showed that replacement reactions were not consistently localized within the rock samples. In some instances, these reactions occurred along the grain boundaries (hydroxylapatite replacing calcite in 0.1 M Na-phosphate solution; Fig. 6a, b), while in others, the external surfaces of the cubes were predominantly affected (Mg-carbonates and Mg-hydroxides replacing calcite in seawater, and hydroxylapatite replacing calcite in 1 M Na-phosphate solution; Figs. 3b–d, 6c, d). However, all reactions maintained the original cube dimensions resulting in pseudomorphic replacements. These phenomena were also reported by Pedrosa et al. (2016) using various phosphate solutions and Carrara Marble. With a fixed temperature (200 °C) for every experiment, fluid composition and time were the only two initial variables. Apart from solution composition, reactions would most likely be constrained by kinetics and the random nature of the 3-dimensional grain boundary networks. Repetition of all experiments indicated the reproducible thermodynamic reactions corresponding to the initial and changing fluid compositions. This was most clearly seen in the replacements formed during the reactions of Carrara Marble and seawater where changing fluid composition controlled the phase that could become supersaturated within the grain boundaries and hence precipitate, as seen in Fig. 3b–d.

Grain boundaries vs. external surfaces of the cube

The experiments showed variations in reaction pathways, either using grain boundaries or reacting at the mineral cube surfaces. These differences can be assessed in terms of fluid composition as well as fluid volume. Phreeqc has been used to elucidate these effects. Figure 10 shows the difference in the saturation indices of the involved phases (from PhreeqC simulations presented in Online Resource 2) after the dissolution of a 1 nm layer of the parent phase, using a volume of fluid that corresponds to the bulk fluid (2 ml) and one that represents the constrained volume of a grain boundary (1 µm). Replacement reactions along grain boundaries were clearly observed in the anorthosite–sodium silicate solution experiments, as well as in the experiments where a 0.1 M sodium phosphate solution was used with Carrara Marble. In these cases, a positive saturation index for the involved phases is only observed when using a grain boundary fluid volume (1 µm) in the PhreeqC simulations (Fig. 10a, b). The clear implication is that solution volume will also control potential replacement reactions.

In the anorthosite experiments both pure water and NaCl solutions showed no changes, either in cube size or grain boundary width, during the time scale of the experiments (3 months). When a sodium silicate solution was used in the anorthosite experiments the reaction was only observed after 3 months. Labradorite will be more soluble than albite in a sodium silicate solution at high pH values (Hövelmann et al. 2010), favoring a continuous labradorite dissolution until albite supersaturation is reached. Simulations show higher solubility values for albite than labradorite (Fig. 9a) but results might be limited by the available thermodynamic parameters that could not reflect our experimental conditions. The higher saturation index of albite in the constrained grain boundary fluid, compared with the bulk fluid, might enhance the replacement along the grain boundaries rather than on the external surface of the cube, which agrees with the experimental results (Fig. 7) where replacement was only observed along the grain boundaries. Albite growth will be followed by a chemical equilibration as is observed in the element maps in Fig. 4e–h and Table 1 showing more sodic albite cores and Na-poorer rims. The formation of albite from the coupling of labradorite dissolution and albite precipitation at 200 °C is remarkable and confirms the dissolution–precipitation mechanism because at this relatively low temperature solid state diffusion would be far too slow. Previous studies have been made at > 600 °C (Hövelmann et al. 2010 and references therein).

For the replacement of Carrara Marble by hydroxylapatite two different replacement patterns were observed: a 0.1 M Na phosphate (Na_2HPO_4) solution produced only replacement along the grain boundaries (Fig. 6a, b); while a 1 M solution resulted in the replacement occurring from the external surfaces of the cube and affected only the outer most grain boundaries (Fig. 6c, d). In both cases, the replacement was already visible after 5 days. Supersaturation of hydroxylapatite within a calcite-fluid boundary layer could be quickly achieved because of its low solubility in the solution. Lower Na_2HPO_4 concentrations might need an effective interfacial boundary layer to produce a replacement reaction and the tight space along the grain boundaries could enhance the reaction preventing the dissolved Ca^{2+} ions from diffusing away from this interface.
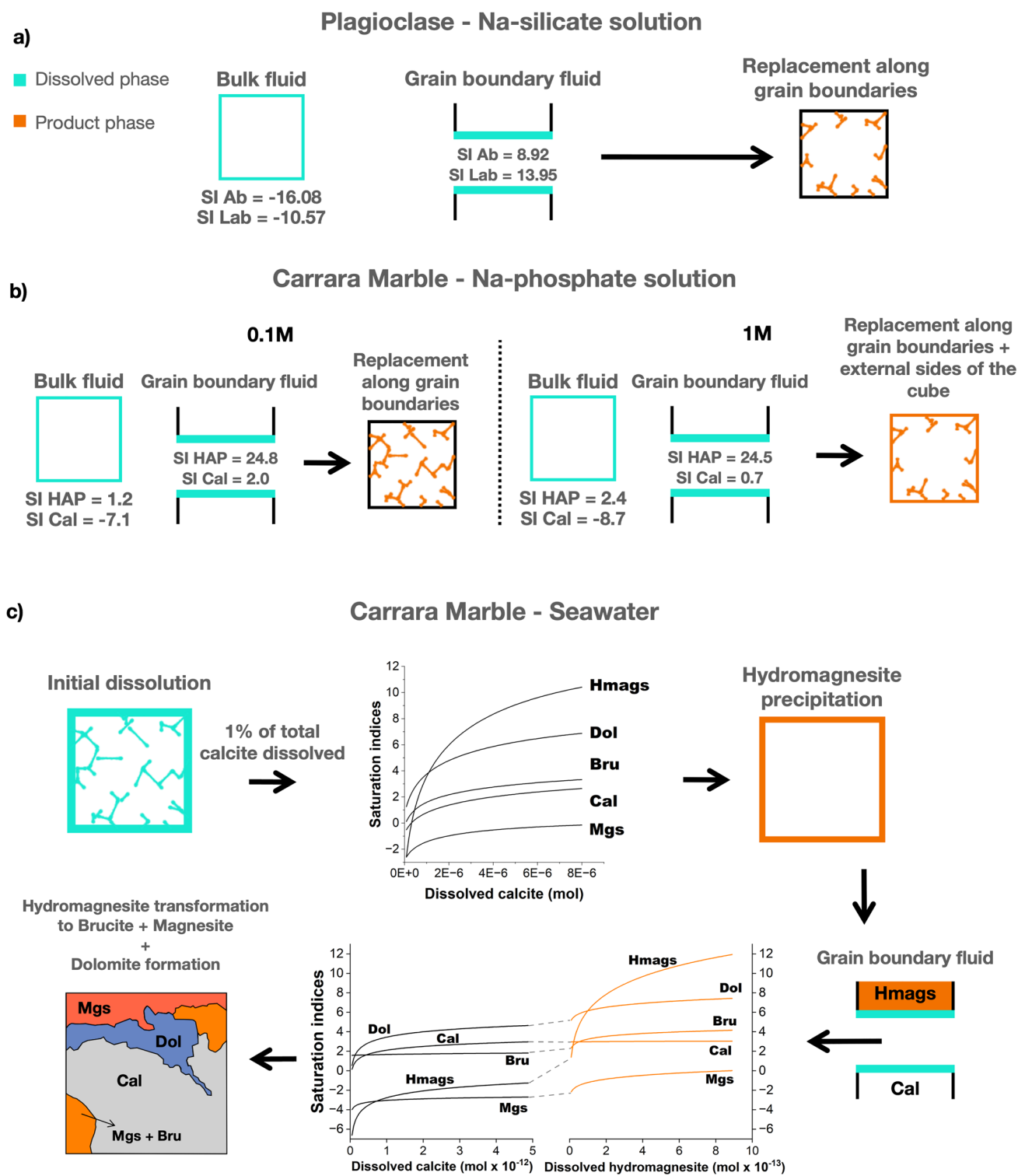
Fig. 10 Series of models after experimental observations and PhreeqC simulations (Online Resource 2). In **a** and **b** 1 nm wide layer in the Carrara Marble and anorthosite rock cube was dissolved through simulations to show the different SI (Saturation Indices) of the involved phases in the bulk fluid and in a 1 μm wide grain boundary. See text for implications in the reaction pathways. c) Evolution of the Carrara Marble–seawater system. In this simulation, 1% of the total Carrara Marble cube was dissolve to plot the SI evolution of the involved phases, as a result a layer of hydromagnesite precipitates by replacement around the cube surface in contact with the bulk solution. Then, we simulated the SI evolution in a grain boundary formed by a grain of calcite and another grain of hydromagnesite to illustrate in the last image the final replacement products observed after SEM and microprobe analyses

The higher saturation index of hydroxylapatite in the grain boundary fluid compared with the bulk fluid when simulating in PhreeqC dissolving a 1 nm layer of calcite (Fig. 10b) reflects the enhancing effects of grain boundaries for fluid–rock reactions. By increasing phosphate concentration, supersaturation might be reached faster at wider interface boundary layers and precipitation of hydroxylapatite can occur at the bulk fluid–mineral interface.

Kinetic control on product phase precipitation

To reflect the strong initial dissolution of calcite in the seawater experiments, simulations in PhreeqC dissolving 1% of the total Carrara Marble cube were performed (Fig. 10c). The possible number of involved phases when using this solution with Carrara Marble are more than in the other experiments. As shown in the simulations (Online Resource 2), following the initial 10 to 20-day period characterized by calcite dissolution, the supersaturated phases that could replace calcite included hydromagnesite, dolomite, and brucite. In this scenario, kinetics plays a strong role so that the phase with the fastest precipitation rate, that is, the first to reach supersaturation, controls the initial replacement process. The saturation index of hydromagnesite increases more rapidly in response to calcite dissolution compared to the other phases involved (Fig. 10c). This, coupled with the fast kinetic rate of hydromagnesite precipitation (Hänchen et al. 2008), enables this phase to quickly replace calcite on the external surfaces of the cube, consuming Mg^{2+} and hindering the reaction from taking place along grain boundaries. Upon precipitation of the first Mg-phase layer, ion supply from the bulk fluid to the internal grain boundaries is consequently interrupted, resulting in control of subsequent reactions along the grain boundaries. As can be seen in Fig. 3b–d, other minor phases, such as Ca-sulphate, precipitated only along grain boundaries.

Chloride-bearing solutions might also enhance the overall reaction process (Winkler and Lüttge 1999; Pedrosa 2016). This is clearly observed by the higher porosity estimations observed for the samples reacted with a NaCl solution in comparison with just pure water (Fig. 2; Table 3; Online Resources 1). For a replacement process, the Cl^- ions present in the seawater could accelerate the nucleation rates (Winkler and Lüttge 1999) which will be reflected in the hydromagnesite precipitating on the cube's surface, where the source of Cl^- ions is higher. While on the grain boundaries, the recently dissolved calcite could decrease the Cl^- ratio in solution until the solution is completely homogenized.

Reaction front propagation

Generation of an interconnected porosity in the product phase is essential for maintaining a fluid pathway within a reacting mineral and is mainly controlled by: (1) molar volume changes between parent mineral and new product phases, and (2) the relative solubilities of the parent and product phases (Pollok et al 2011). During an interface-coupled dissolution precipitation replacement, an effective fluid pathway, required for the progression of the reaction front towards the core of the parent grains, can arise through two possible pathways: (1) newly formed interconnected pores or, (2) reaction-induced fracturing, due to a large molar volume increase during the replacement reaction (Jamtveit et al. 2009; Plümper et al. 2012). Resulting from this coupled dissolution and precipitation, elements are mobilized so that ionic species not reprecipitated will be carried in the aqueous phase to be possibly involved in subsequent reactions. The relatively high temperatures used in our experiments (200 °C) might affect initial grain boundary cracking (Raghami et al. 2020; Zhang et al. 2021), especially in areas with more internal stresses such as triple points and grain vertices.

As porosity is observed in all of our replacement reactions, as seen in Figs. 3, 6, and 7, the relative solubilities between the parent and product phase should play an important role (Pollok et al. 2011). When Carrara Marble reacts with seawater, interconnected porosity within the first precipitated layer would have been effective enough to allow Mg^{2+} ions to diffuse within the aqueous fluid from the bulk fluid to inner parts of the grains. Within the pores, the fluid composition would locally vary while the pores are used as the connecting pathway between the bulk fluid, the mineral-fluid boundary layer and the parent phase, driven by the need to achieve compositional equilibration. Once chemical equilibration begins and pores are formed, then textural equilibration will inevitably follow to attempt to reach a lower energetic state (Putnis et al. 2005). This local variability might be responsible for the pore size distribution along the replacement reaction pathway.

Assuming no significant changes in porosity of the product phase, the replacement of calcite by hydroxylapatite produces a reduction in the molar volume of $\Delta V = -14\%$. Considering extensive porosity development can be observed in the precipitated hydroxylapatite (Fig. 3f, h), and the hydroxylapatite Raman spectra show carbonate peaks (Online Resource 3), we could assume that the density of the product phase will be considerably lower than the one known for solid hydroxylapatite ($\rho = 3.16$ g/cm^3) and, therefore, the reaction will probably produce an increase in the molar volume. Reaction-induced fracturing as that reported during serpentization in Plümper et al. (2012) was not observed in the Carrara Marble experiments. In this case,

the relative solubilities between calcite and hydroxylapatite might be key, the latter being highly insoluble compared with calcite (SI HAP = 1.2, SI Cal = − 7.1; saturation indices for hydroxylapatite and calcite calculated with PhreeqC in Online Resource 2 and Fig. 10b). Dissolution of calcite must be faster than or equal to the precipitation rate of hydroxylapatite to allow for a reaction front to progress, generating porosity, and compensate for possible molar volume increase. The presence of a gap between the product and parent phase (Fig. 6b) might also indicate a difference in the relative solubilities but we cannot exclude the fact that this gap might be a quenching effect. Porosity generation is observed at the micron scale as elongated pores close to the grain boundaries and smaller rounded pores close the reaction front, similar to the ones observed in Pedrosa et al. (2016), with calcite and Ca-phosphate phases also involved. This porosity evolution is probably related to a textural equilibration that allows initially formed rounded small pores to interconnect, creating elongated larger pores, hence allowing fluid permeation.

The replacement reaction front is smoother when using 1 M Na_2HPO_4 solution instead of the 0.1 M Na-phosphate solution (Fig. 6c, d). By increasing 10 times the molar concentration of the solution, the kinetic rate of the replacement reaction should be higher, producing smoother reaction fronts as has been shown in previous models (Koehn et al. 2021), but local compositional variations in the pore fluid present a significant challenge in the devolvement of accurate reaction front propagation models in fluid-driven replacements reactions (Molins et al. 2021; Spurin et al. 2021).

Since the molar volumes of albite and labradorite are very similar, the relative solubilities between the product and parent phases will be the driving factor allowing porosity generation (Hövelmann et al. 2010). Pores in the precipitated albite (nm- scale) are not as big as in the Carrara Marble experiments (nm- and µm- scale) and were not resolvable by SEM, but the reaction front propagation (Fig. 7) indicates that interconnected porosity had to be present, as shown by Hövelmann et al. (2010) from TEM imaging. A non-effective interconnected porosity development might limit the chances of reaction front propagation and could explain why the extent of the replacement was much less in the other runs of experiments than in the first run at 3 months. Previous experiments show very similar results when using crystal powder or rock samples as starting materials (Lüttge and Metz 1993). With conditions as the ones used in our experiments where the replacement reactions are not always likely to occur, important factors such as the available surface area or the internal heterogeneities of a crystal might play a critical role (Lange 2021). Further longer time experiments are needed to confirm and extend an understanding of these results but are out of the initial scope of this research.

Replacement reactions in silicate rock-forming minerals such as plagioclase are slow at 200 °C but our experiments confirm that mineral replacements are possible under conditions compatible with sedimentary and diagenetic processes.

Further reactions in the seawater—marble system

In the seawater—marble system at 200 °C, hydromagnesite might be the first phase to precipitate, as the PhreeqC simulations suggest (Fig. 10c), and will be controlled by the kinetics of the system and the solution availability at the mineral—bulk fluid interface, producing a replacement along the external surfaces of the cube. Consequently, the fluid will be depleted in Mg ions so that along the grain boundaries, the fluid composition cannot become supersaturated enough to form hydromagnesite. Because the initial surface replacement reduces the supply of Mg^{2+} ions from the original bulk solution into the grain boundaries of the rock, calcite will dissolve and reprecipitate as is observed by the narrowing of the grain boundaries after 20 days. Similar to the cyclic behaviour observed with Carrara Marble in pure water and NaCl solutions, reprecipitated calcite along the grain boundaries will eventually redissolve. Such process will probably generate porosity in the reprecipitated calcite but this has not been observed on the BSE images. The use of higher resolution techniques that could identify the presence of nanopores are needed to verify this process.

From the Raman spectra of magnesite ($MgCO_3$) and brucite ($Mg(OH)_2$)—magnesite intergrowth (Online Resource 3) present in the replacement of calcite by Mg-phases, we deduce that the initial hydromagnesite will eventually be replaced by other phases (Hänchen et al. 2008) as the composition of the fluid dynamically changes. An increase in the ionic strength coupled with a decrease in the magnesium concentration promotes the transformation rate of hydromagnesite to magnesite (Zhang et al. 2000). Therefore, under conditions of low magnesium concentration, hydromagnesite dehydration may lead to the generation of magnesite and brucite. Restricting the availability of Mg ions from the bulk fluid also results in decreased Mg levels in the solution entrapped within the cube, facilitating new reactions and yielding an outer layer of magnesite, followed by a layer of magnesite and brucite intergrowths in contact with the original calcite. The combined effect of consuming the magnesium supply, hence reducing Mg ions in the solution, and increasing the calcium content of the solution will eventually allow dolomite precipitation close to the reaction front as can be seen in Fig. 3d. This is also supported by the MgO and CaO mol% variations through the replacement profile (Fig. 5). Elevated Mg concentration could support a mechanism involving hydromagnesite dissolution and subsequent magnesite precipitation. In our experiments, this process may be occurring on the hydromagnesite grains in

contact with the bulk fluid (Fig. 10c). The whole system is seen to be highly dynamic as expected from the nature of a coupled dissolution–precipitation reaction because the solution composition is constantly changing and therefore allowing for continued new reactions to occur. We have analyzed randomly chosen sections of reacted rock cubes but reactions will occur in 3-dimensions within the grain boundaries in both advancing and retreating directions. The replacement of calcite by Mg-carbonates and Mg-hydroxides during hydrothermal experiments using enriched Mg^{2+} solutions has been previously reported (e.g., Duan et al. 2021; Etschmann et al. 2014; Jonas et al. 2015). Our experimental results confirm previous research as well as extending an understanding of reactive-fluid pathways within nominally solid rocks.

Conclusions

This study demonstrates the complex and dynamic nature of interface-coupled dissolution–precipitation processes in both carbonate and silicate rock systems, the two most common rock-forming minerals. The role of grain boundaries, fluid composition, and the relative solubilities of parent and product mineral phases are crucial in determining the replacement reactions that take place. Our experiments have shown that these reactions can vary spatially, occurring along grain boundaries or the external surfaces of the rock cube that in nature could represent a wide-open fracture, and can be influenced by factors such as fluid volume and reaction kinetics.

The observed cyclic behavior of dissolution and reprecipitation, particularly in the Carrara Marble experiments, highlights the dynamic nature of these systems. The interplay between fluid composition, supersaturation, and the precipitation rates of different phases may lead to a sequence of reactions, ultimately resulting in the formation of multiple product phases. This complexity is further emphasized by the generation of porosity and propagation fronts, which require effective fluid pathways and depend on factors such as molar volume changes and the relative solubilities of the involved minerals.

By recognizing the importance of grain boundaries, fluid composition, and reaction kinetics in these processes, we can better predict the behavior of natural systems, including those related to sedimentary and diagenetic settings, as well as fluid-induced metamorphic reactions, and therefore improve our ability to interpret the complex reactions that occur within them. Mineral grains decorating grain boundaries may enable us to interpret the previous presence of specific fluid compositions that would allow for potential coupled reactions and the formation of these new phases.

Furthermore, the reactions reported here are not limited to the rock types chosen for study but should also equally apply to all multimineralic rock types. By understanding fluid–mineral interactions in monomineralic rocks we can begin to approach an understanding of potential fluid–rock interactions through grain boundaries, as well as more open fractures and pores, existing in real Earth scenarios. Coupled dissolution–precipitation reactions observed at grain boundaries on a µm scale can equally apply to large-scale rock masses exposed to aqueous fluid infiltration in natural environments.

Declarations

References

Brugger J, Liu W, Etschmann B, Mei Y, Sherman DM, Testemale D (2016) A review of the coordination chemistry of hydrothermal systems, or do coordination changes make ore deposits? Chem Geol 447:219–253. https://doi.org/10.1016/j.chemgeo.2016.10.021

Drüppel K, Wirth R (2018) Metasomatic replacement of albite in nature and experiments. Minerals 8(5):214. https://doi.org/10.3390/min8050214

Duan G, Brugger J, Etschmann B, Ram R, Frierdich A, Micklethwaite S (2021) Formation of Mg-carbonates and Mg-hydroxides via calcite replacement controlled by fluid pressure. Contrib Min Petrol. https://doi.org/10.1007/s00410-020-01755-4

Etschmann B, Brugger J, Pearce MA, Ta C, Brautigan D, Jung M, Pring A (2014) Grain boundaries as microreactors during reactive fluid flow: experimental dolomitization of a calcite marble. Contrib Mineral Petrol 168(2):1–12. https://doi.org/10.1007/s00410-014-1045-z

Fyfe WS, Price NJ, Thompson AB (1978) Fluids in the earth's crust: their significance in metamorphic, tectonic, and chemical transport processes. Elsevier Scientific Pub Co, UK

Hänchen M, Prigiobbe V, Baciocchi R, Mazzotti M (2008) Precipitation in the Mg-carbonate system-effects of temperature and CO2

pressure. Chem Eng Sci 63(4):1012–1028. https://doi.org/10.1016/j.ces.2007.09.052

Hövelmann J, Putnis A, Geisler T, Schmidt BC, Golla-Schindler U (2010) The replacement of plagioclase feldspars by albite: observations from hydrothermal experiments. Contrib Mineral Petrol 159(1):43–59. https://doi.org/10.1007/s00410-009-0415-4

Jamtveit B, Putnis CV, Malthe-Sørenssen A (2009) Reaction induced fracturing during replacement processes. Contrib Mineral Petrol 157(1):127–133. https://doi.org/10.1007/s00410-008-0324-y

Janssen A, Putnis A, Geisler T, Putnis CV (2010) The experimental replacement of ilmenite by rutile in HCl solutions. Mineral Mag 74(4):633–644. https://doi.org/10.1180/minmag.2010.074.4.633

Jonas L, John T, King HE, Geisler T, Putnis A (2014) The role of grain boundaries and transient porosity in rocks as fluid pathways for reaction front propagation. Earth Planet Sci 386:64–74. https://doi.org/10.1016/j.epsl.2013.10.050

Jonas L, Müller T, Dohmen R, Baumgartner L, Putlitz B (2015) Transport-controlled hydrothermal replacement of calcite by Mg-carbonates. Geology 43(9):779–783. https://doi.org/10.1130/G36934.1

Julia M, Putnis CV, King HE, Renard F (2023) Coupled dissolution-precipitation and growth processes on calcite aragonite and Carrara marble exposed to cadmium-rich aqueous solutions. Chem Geol 621:121364. https://doi.org/10.1016/j.chemgeo.2023.121364

Kish L, Cuney M (1981) Uraninite-albite veins from the mistamisk valley of the labrador trough. Quebec Min Mag 44(336):471–483. https://doi.org/10.1180/minmag.1981.044.336.13

Koehn D, Piazolo S, Beaudoin NE, Kelka U, Spruženiece L, Putnis CV, Toussaint R (2021) Relative rates of fluid advection, elemental diffusion and replacement govern reaction front patterns. Earth Planet Sci. https://doi.org/10.1016/j.epsl.2021.116950

Kruhl JH, Wirth R, Morales LFG (2013) Quartz grain boundaries as fluid pathways in metamorphic rocks. J Geophys 118(5):1957–1967. https://doi.org/10.1002/jgrb.50099

Labotka TC, Cole DR, Fayek M, Riciputi LR, Stadermann FJ (2004) Coupled cation and oxygen-isotope exchange between alkali feldspar and aqueous chloride solution. Am Mineral 89(11–12):1822–1825. https://doi.org/10.2138/am-2004-11-1229

Lange I, Toro M, Arvidson RS, Kurganskaya I, Luttge A (2021) The role of crystal heterogeneity in alkali feldspar dissolution kinetics. Geochim Cosmochim Acta 309:329–351. https://doi.org/10.1016/j.gca.2021.06.032

Lüttge A, Metz P (1993) Mechanism and kinetics of the reaction: 1 dolomite + 2 quartz = 1 diopside + 2CO$_2$: a comparison of rock-sample and of powder experiments. Contrib to Mineral Petrol 115:155–164. https://doi.org/10.1007/BF00321217

Molins S, Soulaine C, Prasianakis NI et al (2021) Simulation of mineral dissolution at the pore scale with evolving fluid-solid interfaces: review of approaches and benchmark problem set. Comput Geosci 25(4):1285–1318. https://doi.org/10.1007/s10596-019-09903-x

Niedermeier DRD, Putnis A, Geisler T, Golla-Schindler U, Putnis CV (2009) The mechanism of cation and oxygen isotope exchange in alkali feldspars under hydrothermal conditions. Contrib Mineral Petrol 157(1):65–76. https://doi.org/10.1007/s00410-008-0320-2

Oliver NHS, Cleverley JS, Mark G et al (2004) Modeling the role of sodic alteration in the genesis of ion oxide-copper-gold deposits, Eastern Mount Isa Block. Australia Econ Geol 99(6):1145–1176. https://doi.org/10.2113/gsecongeo.99.6.1145

Parkhurst DL, Appelo CAJ (1999) User's guide to PHREEQC (Version 2): a computer program for speciation, batch-reaction, one-dimensional transport, and inverse geochemical calculations. Water-Res Invest Rep. https://doi.org/10.3133/wri994259

Pedrosa ET, Putnis CV, Putnis A (2016) The pseudomorphic replacement of marble by apatite: the role of fluid composition. Chem Geol 425:1–11. https://doi.org/10.1016/j.chemgeo.2016.01.022

Pedrosa ET, Boeck L, Putnis CV, Putnis A (2017) The replacement of a carbonate rock by fluorite: kinetics and microstructure. Am Mineral 102(1):126–134. https://doi.org/10.2138/am-2017-5725

Petráňová V, Valach J, Viani A, Estébanez MP (2016) Determination of thermal response of Carrara and Sneznikovsky marble used as a building materials. Acta Polytech CTU Proc 3:56–59. https://doi.org/10.14311/app.2016.3.0056

Plümper O, Røyne A, Magrasó A, Jamtveit B (2012) The interface-scale mechanism of reaction-induced fracturing during serpentinization. Geology 40(12):1103–1106. https://doi.org/10.1130/G33390.1

Pollok K, Putnis CV, Putnis A (2011) Mineral replacement reactions in solid solution-aqueous solution systems: Volume changes, reactions paths and end-points using the example of model salt systems. Am J Sci 311(3):211–236. https://doi.org/10.2475/03.2011.02

Putnis A (2021) Fluid-mineral interactions: controlling coupled mechanisms of reaction, mass transfer and deformation. J Petrol. https://doi.org/10.1093/petrology/egab092

Putnis A, Putnis CV (2007) The mechanism of reequilibration of solids in the presence of a fluid phase. J Solid State Chem 180(5):1783–1786. https://doi.org/10.1016/j.jssc.2007.03.023

Putnis CV, Putnis A (2022) A mechanism of ion exchange by interface-coupled dissolution-precipitation in the presence of an aqueous fluid. J Cryst Growth. https://doi.org/10.1016/j.jcrysgro.2022.126840

Putnis CV, Ruiz-Agudo E (2021) Nanoparticles formed during mineral-fluid interactions. Chem Geol 586:120614. https://doi.org/10.1016/J.CHEMGEO.2021.120614

Putnis CV, Tsukamoto K, Nishimura Y (2005) Direct observations of pseudomorphism: compositional and textural evolution at a fluid-solid interface. Am Mineral 90(11–12):1909–1912. https://doi.org/10.2138/am.2005.1990

Putnis CV, Geisler T, Schmid-Beurmann P, Stephan T, Giampaolo C (2007) An experimental study of the replacement of leucite by analcime. Am Mineral 92(1):19–26. https://doi.org/10.2138/am.2007.2249

Raghami E, Schrank C, Kruhl JH (2020) 3D modelling of the effect of thermal-elastic stress on grain-boundary opening in quartz grain aggregates. Tectonophysics. https://doi.org/10.1016/j.tecto.2019.228242

Roduit N (2023) JMicroVision: Image analysis toolbox for measuring and quantifying components of high-definition images. Version 1.3.2. https://jmicrovision.github.io (accessed 23 June 2023)

Ruiz-Agudo E, Putnis CV, Putnis A (2014) Coupled dissolution and precipitation at mineral-fluid interfaces. Chem Geol 383:132–146. https://doi.org/10.1016/j.chemgeo.2014.06.007

Smith M, Coppard J, Herrington R, Stein H (2007) The geology of the Rakkurijärvi Cu-(Au) prospect, norrbotten: a new iron oxide-copper-gold deposit in Northern Sweden. Econ Geol 102(3):393–414. https://doi.org/10.2113/gsecongeo.102.3.393

Spurin C, Bultreys T, Rücker M et al (2021) The development of intermittent multiphase fluid flow pathways through a porous rock. Adv Water Resour 150:103868. https://doi.org/10.1016/j.advwatres.2021.103868

Uno M, Koyanagawa K, Kasahara H, Okamoto A, Tsuchiya N (2022) Volatile-consuming reactions fracture rocks and self-accelerate fluid flow in the lithosphere. Earth Planet. https://doi.org/10.1073/pnas.2110776118

Weber J, Starchenko V, Ilavsky J et al (2023) Grain boundary widening controls siderite (FeCO3) replacement of

limestone (CaCO3). Sci Rep 13(1):4581. https://doi.org/10.1038/s41598-023-30757-y

Winkler U, Lütgge A (1999) The influence of $CaCl_2$ on the kinetics of the reaction 1 tremolite + 3 calcite + 2 quartz = 5 diopside + 3 CO_2 + 1 H_2O. Exp Invest Am J Sci 299:393–427. https://doi.org/10.2475/ajs.299.5.393

Xia F, Brugger J, Chen G et al (2009) Mechanism and kinetics of pseudomorphic mineral replacement reactions: A case study of the replacement of pentlandite by violarite. Geochim Cosmochim Acta 73(7):1945–1969. https://doi.org/10.1016/j.gca.2009.01.007

Zhang P, Anderson H, Kelly J, Krumhansl J, Papenguth H (2000) Kinetics and mechanisms of formation of magnesite from hydromagnesite in brine. Technical Report SAN099–19465, Sandia National Laboratories, Albuquerque, NM 87185–0750, USA.

Zhang Y, Francois N, Henley R et al (2021) 3D quantification of microcracks and porosity with respect to brittle failure. 55th US. Rock Mechanics/Geomechanics Symposium.

Zhao XF, Zhou MF (2011) Fe–Cu deposits in the Kangdian region, SW China: a Proterozoic IOCG (iron-oxide–copper–gold) metallogenic province. Miner Deposita 46(7):731–747. https://doi.org/10.1007/s00126-011-0342-y